Optimization of Plasmonic Nano-Antennas

Kursat Sendur, Orkun Karabasoglu, Eray Abdurrahman Baran, and Gullu Kiziltas
Sabanci University, Istanbul, 34956, Turkey

ABSTRACT

The interaction of light with plasmonic nano-antennas is investigated. First, an extensive parametric study is performed on the material and geometrical effects on dipole and bow-tie nano-antennas. The transmission efficiency is studied for various parameters including length, thickness, width, and composition of the antenna as well as the wavelength of incident light. The modeling and simulation of these structures is done using 3-D finite element method based full-wave solutions of Maxwell's equations. Next, a modeling-based automated design optimization framework is developed to optimize nano-antennas. The electromagnetic model is integrated with optimization solvers such as gradient-based optimization tools and genetic algorithms.

INTRODUCTION

Nano-optical applications, such as scanning near-field optical microscopy [1] and data storage [2], require intense optical spots beyond the diffraction limit. Nano-antennas [3-4] can obtain very small optical spots, but their ability to obtain optical spots beyond the diffraction limit is not sufficient for practical applications. In addition to a very small optical spot, a nano-antenna should provide high transmission efficiency for practical applications. The transmission efficiency of a nano-antenna determines the data transfer rate of storage devices and scan times of near-field optical microscopes. Therefore, the efficiency of nano-antennas should be optimized for potential utilization in practical applications. Optimization of nano-antennas is crucial for understanding their potential and limitations for emerging plasmonic applications.

The interaction of antennas with electromagnetic waves has been thoroughly investigated at microwave frequencies. Scaling and optimization rules do not apply at optical frequencies [4]. At visible and infrared frequencies the underlying physics of the interaction of light with metallic nano-antennas is complicated due to the behavior of metals as strongly coupled plasmas [5-8]. Experimental studies have shown light localization using both dipole [9] and bow-tie [10] nano-antennas. A brute-force optimization study of these structures is not practical due to large number of parameters. There is a need for a systematic optimization of these structures.

In this study, we develop a modeling-based automated design optimization framework to optimize nano-antennas. The modeling and simulation are done using 3-D finite element method (FEM), which is integrated with optimization solvers such as genetic algorithms and gradient based optimization tools. First, an extensive parametric study is performed on the material and geometrical effects. Then the proposed design framework is used to optimize nano-antennas.

DIPOLE AND BOW-TIE PLASMONIC NANO-ANTENNAS

To couple incident electromagnetic energy with small scale electronic devices, antennas have been utilized. The antennas achieve this coupling by localizing the incident radiation to smaller dimensions than the wavelength. This coupling mechanism has been well understood for radio frequency and microwave applications, and is also applicable to nano-antennas operating at optical frequencies. At optical frequencies nano-scale metallic antennas can be utilized to couple incident optical beams to length scales much smaller than the diffraction limit.

An antenna is composed of metallic parts. For example, the dipole antenna shown in Fig. 1 (a) is composed of two metallic rods separated by a distance, G. Similarly, a bow-tie antenna shown in Fig. 1 (b) is composed of two triangular metallic pieces, which are also separated by a distance, G. The incident electromagnetic wave creates induced currents on the antenna surface. These induced currents are the source of charge accumulation at the ends of the antenna. If the incident polarization is along the long-axis of the antenna, then the charges of opposite sign are created across the gap separating the metallic parts. The oscillation of the charge is the main source of a localized near-field electromagnetic radiation. This localized radiation is composed of propagating and evanescent components. If a structure is brought in the near-field of this gap, then the radiating fields due to this charge oscillation interact with the structure, which leads to interesting applications, including near-field optical microscopy [1] and data storage [2].

(a)   (b)
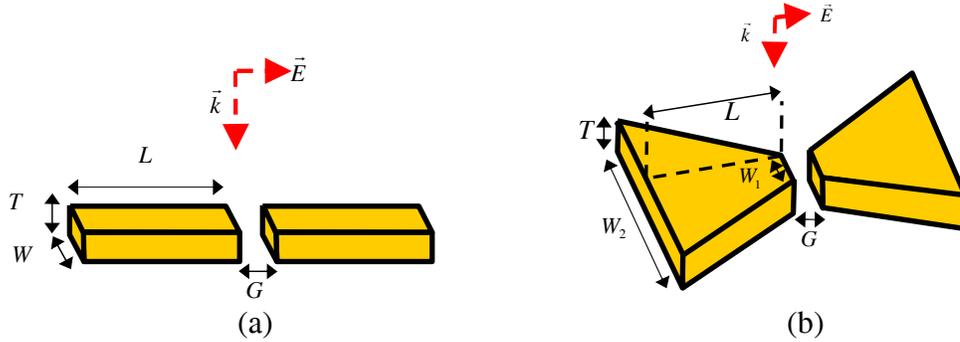
Figure 1. A schematic illustration of a (a) dipole and (b) bow-tie antenna, and their dimensions. The antennas are illuminated with incident electromagnetic radiation shown with $\vec{E}$.

At visible and infrared frequencies, however, the underlying physics of the interaction of light with metallic nano-antennas is complicated due to the behavior of metals as strongly coupled plasmas [5-8]. If the shape and composition of the metallic structures and the wavelength of the incident radiation is appropriately chosen, then it is possible to excite surface plasmon resonances over these metallic particles [11]. Size and shape-dependent surface plasmon resonances of nano-particles can be excited if the frequency of the incident radiation matches the frequency of the oscillation frequency of the free-electron gas of metals.

Surface plasmon resonances are associated with high electric field enhancement. This field enhancement is of particular interest for applications that require high transmission efficiencies in addition to small optical spots. One way to further enhance the electromagnetic near-field radiation is to utilize sharp tips. Due to the lightning rod effect around the sharp tips, the electric field enhancement, and therefore the transmission efficiency of the nano-antenna can be further improved. Therefore, the sharp tips of the bow-tie antenna should provide better field improvement compared to the dipole antenna. However, for a more realistic simulation the bow-tie antennas are modeled as shown in Fig. 1, where the sharp tips are truncated at a width of W_1.

We performed numerical simulations using the FEM to understand the effect of various parameters on the near-field radiation of nano-antennas. Radiation boundary conditions are used in FEM simulations. Tetrahedral elements are used to discretize the computational domain. On the tetrahedral elements, edge basis functions, and second-order interpolation functions are used to expand the functions. Adaptive mesh refinement is used to improve the coarse solution regions with high field intensities and large field gradients. The optical properties of metals used in this study are retrieved from the literature [12]. In Fig. 2 (a), electric field distribution for a dipole antenna is shown on the x-z cut-plane plane, which passes through the center of the antenna. The incident field is polarized in the x-direction, and is propagating in the negative z-

direction. The wavelength of the incident light is 850 nm. The result shows a confined electric field close to the gap region of the antenna. Also a large electric field enhancement is observed. For this simulation, the sizes of the antenna are L= 110, T= 20, W= 20, and G= 20 nm. The magnitude of the incident field is 1 V/m for this calculation. The result suggests that the intensity enhancement at the center of the antenna is over 1000.

In Fig. 2 (b) we next plot the intensity, $|E|^2$ as a function of the length of the antenna. To achieve this plot, we simulated the near-field radiation from the antenna for different antenna lengths, and recorded the electric field values as shown in Fig. 2. (b). The results suggest that the optimum length is around 90 nm when the incident wavelength is 850 nm. Note that the length is for one of the metallic rods. Including the gap and the other rod, the entire length is 200 nm.
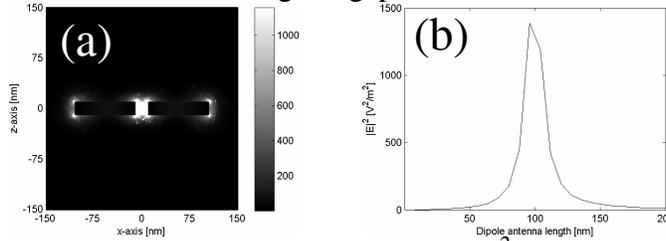
Figure 2. (a) The intensity distribution, $|E(x, y=0, z)|^2$ on the *x-z* plane for a dipole antenna at a wavelength of 850 nm for L= 110, T= 20, W= 20, and G= 20 nm, and (b) The intensity at the center of the gap $|E(x=0, y=0, z=0)|^2$ is plotted for various L at λ = 850 nm.

A similar calculation is repeated for a bow-tie antenna in Fig. 3 (a). Similar to the previous set of calculations, the electric field distribution for a bow-tie antenna is shown on the x-z cut-plane, which passes through the center of the antenna. The wavelength of the incident field is 850 nm. The dimensions of the bow-tie antenna are L= 100, T= 20, W_1= 20, W_2= 220, and G= 20 nm. The field enhancement is slightly larger than that of the dipole antenna. The magnitude of the incident field is 1 V/m for this calculation. The intensity, $|E|^2$, enhancement at the center of the antenna is larger than 1200 for this simulation. In Fig. 3 (b) we next plot the electric field enhancement as a function of the length of the antenna. The results suggest that the optimum length is 120 nm when the incident wavelength is 850. Note that the length is for one of the triangular structures. Including the gap and the other triangle, the entire length is 260 nm.
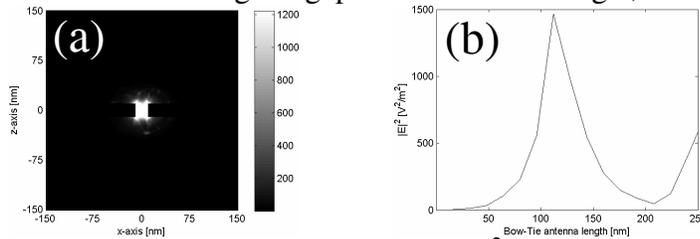
Figure 3. (a) The intensity distribution, $|E(x, y=0, z)|^2$ on the *x-z* plane for a bow-tie antenna at a wavelength of 850 nm for L= 100, T= 20 , W_1= 20 , W_2= 220, and G= 20 nm, and (b) The intensity at the center of the gap $|E(x=0, y=0, z=0)|^2$ is plotted for various L, at a λ = 850 nm.

The electric field is plotted at the center of the antenna as a function of the incident wavelength and antenna length. The incident wavelength is varied from 400 nm to 2000 nm by intervals of 50 nm. At each wavelength, we performed simulations by changing the antenna length. The intensity at the center of the gap, $|E(x=0, y=0, z=0)|^2$, is calculated for each wavelength and antenna length. By recording the intensity over the rectangular grid shown in Fig. 4, we formed the surface graphs. Rather than using a constant incident field, we used a constant power value of 1 mW. The power calculations are based on a focused beam model [13]. In Fig 4 (a), the intensity is plotted as a function of wavelength and antenna length for a gold

antenna with other parameters set as T= 10, W= 10, and G= 20 nm. The optimum wavelength shifts toward longer wavelengths as the antenna length is increased. There is a sharp drop in the intensity enhancement due to surface plasmon damping. Fig 4 (b) shows the results for T= 20, W= 20, and G= 20 nm. Increasing the antenna cross section shifts the optimum wavelengths to smaller values. A similar trend is observed in Fig 4 (c) with T= 50, W= 50, and G= 20 nm. In Fig. 4 it should be noted that the $|E(x=0, y=0, z=0)|^2$ values do not correspond to the intensity enhancement. The magnitude of the incident electric field in not 1 V/m, rather the incident power is selected as 1 mW. Intensity enhancement is still in the order of 1000 as shown in Figs. 2 and 3.


(a)   (b)   (c)
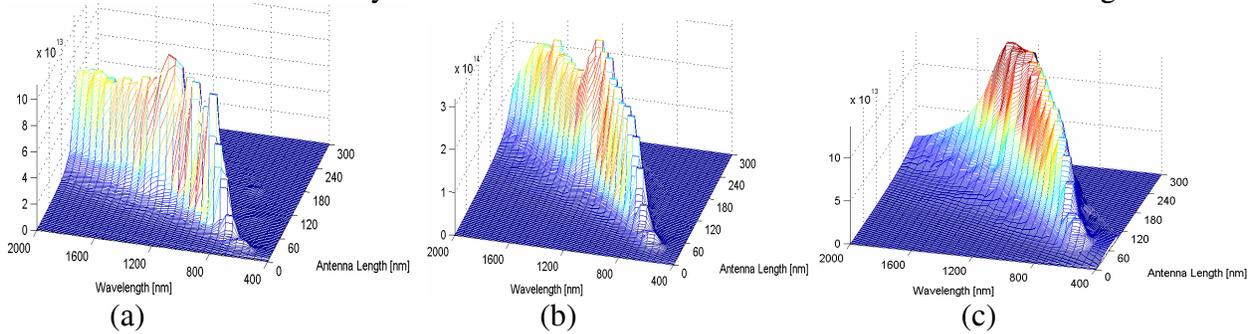
Figure 4. The intensity as a function of wavelength and antenna length for: (a) T= 10, W= 10, and G= 20 nm, (b) T= 20, W= 20, and G= 20 nm, and (c) T= 50, W= 50, and G= 20 nm.

The important parameters in Fig. 4 are the optimum antenna length and the corresponding intensity value at various wavelengths. Figure 5 (a) and (b) illustrate the optimum length and corresponding intensity values extracted from surface plots for gold dipole antennas with various cross sections. In Fig. 5 (a) and (b) the optimum length of the antenna and the corresponding intensity values are plotted as a function of the wavelength. The results in Fig. 5 (a) suggest that the optimum antenna length is longer for thicker antennas. The optimum length and intensity are plotted for a silver dipole antenna as a function of the wavelength in Fig. 6.
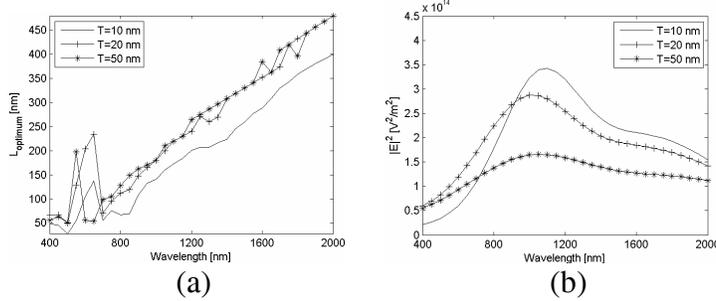

(a)   (b)
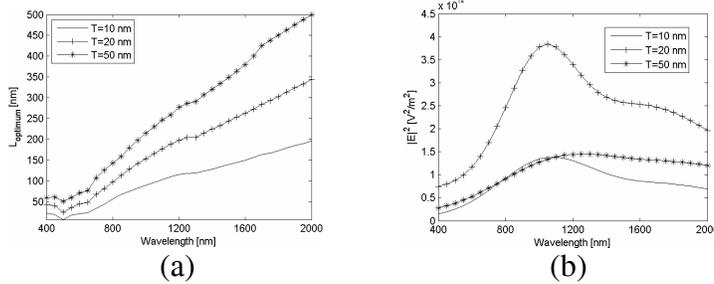
Figure 5. (a) Optimum gold dipole antenna length as a function of wavelength, (b) Optimum intensity values $|E(x, y=0, z)|^2$ for optimum antenna lengths as a function of wavelength.

(a)   (b)
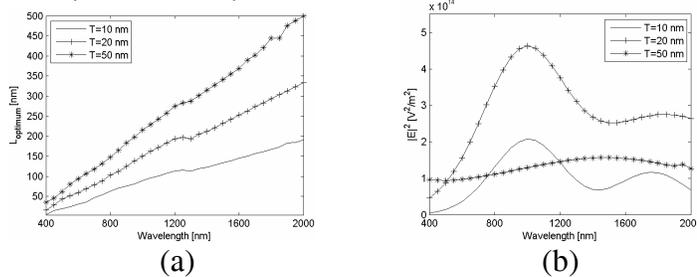
Figure 6. (a) Optimum silver dipole antenna lengths as a function of wavelength, (b) Optimum intensity values $|E(x, y=0, z)|^2$ for optimum antenna lengths as a function of wavelength.

In Fig. 7, the optimum length of a gold bow-tie antenna and the corresponding intensity value at various wavelengths is plotted. The bow-tie antenna parameters are selected as T= 20, W_1= 20, and G= 20 nm. The flare angle is selected as 45°, therefore, the width W_2 corresponds to 20+2*L as the length of the antenna is changed. The results show a trend similar to dipole antennas. The optimum antenna length is, however, longer than that of a dipole antenna. At shorter wavelengths, some unexpected spikes are observed as shown in Fig. 7. In Figs. 2 (b) and 3 (b), if we continue to increase the length of the antenna, we observe further maxima and minima. These spikes correspond to the second optimum length of the antennas. The second and higher optima should provide lower intensity values. However, due to numerical errors, the second maximum gives slightly higher intensity compared to the first maximum at these spikes.


(a)   (b)

Figure 7. (a) Optimum gold bow-tie antenna lengths as a function of wavelength, (b) Optimum intensity values $|E(x, y=0, z)|^2$ for optimum antenna length as a function of wavelength.

OPTIMIZATION FRAMEWORK

The surface plasmon resonances of nano-antennas depend on parameters related to the shape and composition of the nano-antenna as shown in Fig. 1. Complete understanding of surface plasmon resonances of nano-optical systems requires a complete and detailed understanding of possibly many more design parameters, geometries, and material properties. The large number of parameters involved in studying functional plasmonic devices with a brute force numerical parameter simulation is not feasible. To design novel nano-optical transducers a modeling based automated design optimization framework is necessary.

The design framework is formed by integrating a commercial electromagnetic analysis tool Ansoft HFSS with MATLAB's optimization toolbox. Specifically, two different optimization tools are integrated on a MATLAB based scripting interface to iteratively search for optimum geometric parameters of a dipole and bowtie antenna: sequential quadratic programming (SQP) and genetic algorithm (GA). The optimization model consists of maximizing the field intensity $|E(x=0, y=0, z=0)|^2$ subject to bound constraints of [20, 450] and [400 2000] for geometric length and wavelength, respectively. Convergence is achieved in about less than 20 iterations and 10 generations for the SQP and GA framework, respectively. Optimization parameters in the GA setting include 10 individuals, Gaussian Mutation and Roulette Wheel Selection. Optimal lengths for dipole antennas are obtained via SQP, plotted with respect to wavelength, and compared to results obtained via the brute-force simulation in Figure 8. There is an overall agreement except for optimal lengths at wavelengths close to bound constraints. The discrepancies are attributed to two main reasons: Inaccurate brute-force predictions of maximum field intensity of finite sampled frequency points and as expected with gradient based optimization tools, results show that SQP's performance in locating the optimum solution depends on the chosen initial design with especially when the intensity is a multi-modal function. The GA based optimization framework seems to overcome this issue in the expense of

computational time. Optimal results for the bow-tie antenna length converged to 140 nm at 900 nm, and to a dipole length of 286 nm at 1764 nm for a 2 variable optimization study via the GA framework while the SQP was unable to converge for the latter. Initial results seem to be promising in providing the capability of exploring nano-structures with several design parameters. The electric field performance is likely to result in more complicated response functions. Future work includes expanding the framework to hybridize both optimization tools in combining the advantages of global and local optimization tools and to expand the framework to multi-objective design optimization problems.
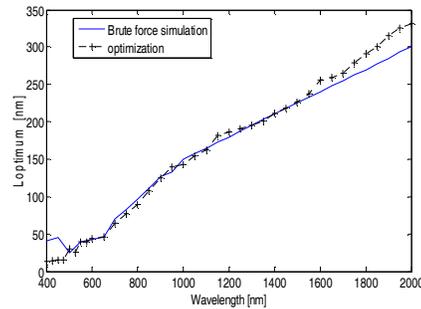
Figure 8. Comparison of the optimization result for a dipole antenna using the SQP method and brute-force simulations.

CONCLUSIONS

In this study, interaction of light with plasmonic nano-antennas was investigated. An extensive study is performed to investigate the effect of the geometric and material properties of nano-antennas on the transmission efficiency. A modeling based automated design optimization framework was also developed. The results of the optimization framework were compared with those of the brute-force simulations.

REFERENCES
1. A. Hartschuh, E. J. Sanchez, X. S. Xie, and L. Novotny, *Phys. Rev. Lett.*, **90**, 095503 (2003).
2. K. Sendur, W. Challener, and C. Peng, *J. Appl. Phys.*, **96**, 2743-2752 (2004).
3. R. D. Grober, R. J. Schoelkopf, and D. E. Prober, *Appl. Phys. Lett.*, **70**, 1354 (1997).
4. L. Novotny, *Phys. Rev. Lett.,* **98**, 266802 (2007).
5. K. Sendur and W. A. Challener, *J. Microsc.*, **210,** 279-283 (2003).
6. H. Raether, *Surface Plasmons on Smooth and Rough Surfaces and on Gratings* (Springer Verlag, 1988).
7. J. J. Burke, G. I. Stegeman, and T. Tamir, *Phys. Rev. B*, **33**, 5186 (1986).
8. H. Raether, *Physics of thin films*, vol. 9, pp. 145-261 (Academic, New York, NY, 1977).
9. P. Muhlschlegel, H.-J. Eisler, O. J. F. Martin, B. Hecht, and D. W. Pohl, *Science*, **308**, 1607-1609 (2005).
10. F. Jackel, A. A. Kinkhabwala, and W. E. Moerner, *Chem. Phys. Lett.*, **446**, 339-343 (2003).
11. K. L. Kelly, E. Coronado, L. L. Zhao, and G. C. Schatz, *J. Phys. Chem. B*, **107**, 668-677 (2003).
12. E. D. Palik, *Handbook of optical constants of solids* (Academic Press, San Diego, CA, 1998).
13. B. Richards and E. Wolf, *Proc. Roy. Soc. London Ser. A*, **253**, 358-379, (1959).